Volume 1 | Number 1 | Jan 2013 | Pages 1–100

# PCCP

Physical Chemistry Chemical Physics
www.rsc.org/pccp

ROYAL SOCIETY OF CHEMISTRY

ROYAL SOCIETY OF CHEMISTRY

www.rsc.org/pccp

# Journal Name

## ARTICLE

# B800-B850 coherence correlates with energy transfer rates in the LH2 complex of photosynthetic purple bacteria

**Cathal Smyth**,[a] **Daniel G. Oblinsky**,[b] and **Gregory D. Scholes,**[b*]

Until recently, no analytical measure of many-body delocalization in open systems had been developed, yet such a measure enables characterization of how molecular excitons delocalize in photosynthetic light-harvesting complexes, and in turn helps us understand quantum coherent aspects of electronic energy transfer. In this paper we apply these measures to a model peripheral light-harvesting complex, LH2 from *Rhodopseudomonas acidophila*. We find how many chromophores collectively contribute to the "delocalization length" of an excitation within LH2 and how the coherent delocalization is distributed spatially. We also investigate to what extent this delocalization length is effective, by examining the impact of bipartite and multipartite entanglement in inter-ring energy transfer in LH2.

## Introduction

The field of quantum biology, or at least the very idea, is nearly as old as quantum mechanics itself. In his 1944 book *"What is life?"*[1] Schrodinger wondered whether quantum mechanics could have a macroscopic impact in molecular biology. Curiously, Schrodinger also coined the term "entanglement" to describe the unusual correlations shared by inseparable quantum states. It is fitting then that the rise of the fields of quantum biology and quantum information emerged at the same time in the mid 1990s. As one community was coming to grips with qubits, quantum algorithms and cryptography, another was excitedly studying the coherent delocalization of excitons in photosynthesis. The 1995 report by [2] on the crystal structure the peripheral light-harvesting complex LH2 (from the purple anoxygenic bacterium *Rhodopseudomonas (Rps.) acidophila* strain 10050) dominated the discussion at a European Science Foundation workshop (organized by Leonas Valkunas and Rienk van Grondelle) held in Birstonas, Lithuania in 1996. One of the principal concerns was the size and duration of coherent excitation in LH2. A collection of papers associated with the workshop containing studies of the delocalization in LH2 and methods of

delocalization measurement can be found in volume 101, issue 37 (1997) of the *Journal of Physical Chemistry B*.

Since 2007 there has been considerable research on long-lived coherence within various light harvesting complexes, such as the Fenna–Mathews–Olson (FMO) complex from green sulfur bacteria [3-5], cryptophyte algae [6-9] at room temperature, as well as in the light-harvesting complex (LHCII) of green plants [10]. Whether this long-lived coherence is of an electronic, a vibrational or hybrid nature remains an open question, and new experimental techniques are needed [11]. Motivated by these experimental results, and making use of the entanglement measures [12-14] developed for quantum information, a large body of work focused on the theory of coherence in energy transfer [15-25]. Not only is electronic coherence seen as an important aid in energy transfer [26], but so too is the surrounding environment [17,27-30].

In order to ascertain the role of quantum coherence in energy transfer, one needs to fully understand its scope; both spatially and temporally. From the inverse participation ratio [18,27,31-34] (IPR), to measures of

bipartite entanglement [15], we have seen great strides in measures that resolve quantum effects, but none that have to date given a proper delocalization length for systems undergoing decoherence. The IPR is an ideal measure of delocalization in pure states, as the wavefunction is known exactly. However, since the IPR is purely a function of state populations and not state coherence, it fails as a measure for an open system. Measures based on bipartite entanglement [15-18] were able to accommodate the added complexity of decoherence. Crucially however, these measures infer the delocalization length by examining the amount of coherence in a system (which is by definition a 2-body or bipartite correlation) rather than explicitly detecting many-body correlations.

Here we present an in-depth analysis of delocalization within LH2 using newly developed analytical delocalization measures based upon multipartite entanglement [35] that detect these many-body correlations. These measures finally allow us to get a true sense of how to visualize the delocalization length in a light harvesting complex such as LH2, and to what level such delocalization plays a role in energy transfer. Within the criteria of these measures, states with a delocalization length of $k$ sites can be considered to have genuine $k$-partite entanglement (where $k \leq n$) as they are not producible by states with $(k-1)$-partite entanglement [36]. In other words, such a state cannot be described as having a delocalization length less than $k$ sites.

This paper is structured in several parts. In section 1 we briefly describe the process of light harvesting within purple bacteria. Section 2 provides the methods used to develop the Hamiltonian, equations of motion, and measures of delocalization. We then apply these measures in section 3 to three different simulations based on the symmetric Hamiltonian, to predict the delocalization length in LH2 as a function of time. The following section considers the physical distance between correlated chromophores, as an alternate method of measuring the delocalization length. Finally in section 5 we study the role of delocalization in energy transfer by using an ensemble of disordered Hamiltonians, and follow with our conclusions.

# 1 Light harvesting in purple bacteria

The purple anoxygenic bacterium *Rps. acidophila* (strain 10050) contains two light harvesting complexes, the core complex LH1 and the peripheral complex LH2. Each light harvesting complex contains one or more rings of bacteriochlorophyll-*a* (Bchl-*a*) molecules that collectively absorb photons, store and transfer this energy to the reaction centre where it is converted to chemical energy [37]. The LH2 complex of *Rps. acidophila* is composed of two spectrally distinct rings: the B800 and B850 rings, so called owing to the wavelength of their peak absorption. This spectral distinction comes largely from the difference in nearest neighbour coupling; The nine B800 Bchl-*a* are weakly coupled ($\sim 30 \text{ cm}^{-1}$) compared to the eighteen B850 Bchl-*a* ($\sim 300 \text{ cm}^{-1}$).

The LH2 complex is assembled from nine subunits comprising three Bchl-*a* molecules, one carotenoid molecule and two protein $\alpha$-helices labeled $\alpha$ and $\beta$. These subunits associate into a ninefold symmetric ring where the B800 chromophores are widely spaced apart with respect to the B850 chromophores, leading to weak coupling within the B800 ring, while the B850 chromophores are strongly coupled.

Electronic energy transfer in the LH2 complex has been widely studied [38]. For the present work the salient features are that excitation flows from the B800 ring to the B850 ring on a timescale of ~1 ps (depending on the species of purple bacteria) and the excitonic coupling among the chromophores in the B850 ring plays a decisive role in expediting this energy transfer. That excitonic delocalization in the acceptor necessitated development of a modified version of energy transfer theory, known as Generalized Förster Theory, in order to account quantitatively for the mechanism and rate [39]. A key assumption of Generalized Förster Theory is that the donor (B800 in this case) and acceptor (B850) are very weakly electronically coupled, so the excitation hops incoherently. Part of the motivation of the present study is to examine that approximation.

# 2 Methods

## 2.1 System Hamiltonian

The system Hamiltonian for the B800-B850 complex was estimated using procedures outlined in refs [39] and [40] for the off-diagonal and diagonal elements of the Hamiltonian, respectively. Due to the close contact of the inter and intra-dimer pairs of the B850 complex both columbic coupling and short range orbital overlap terms needed to be calculated. Site energies of the $\alpha$, $\beta$, and B800 chromophores were then obtained through fitting absorption, circular dichroism, and fluorescence spectra, recorded for the sample at 298 K.

Atomic resolution detail of the chromophores was taken from the X-ray structure model [41] of the complex from *Rps. acidophila* strain 10050, (PDB ID: 1NKZ). The X-ray geometries of the chromophores were refined by a restrained optimization during which dihedral angles were frozen. The structural optimization was carried out using the Gaussian 09 software package [42] at the B3LYP/cc-pvtz level of theory [43-45]. The resulting ground state structures were used in the calculation of the transition density from the ground to first excited state at the configuration interaction singles level of theory with a correlation consistent triple zeta basis set [46].

Inhomogeneous broadening of the spectra was introduced through diagonal disorder in the Hamiltonian, with 2000 unique spectra averaged to generate the final steady-state spectra compared with the experiment. The inhomogeneous broadening was added by a Gaussian random number generator with a full width-half maximum of 160 cm$^{-1}$ for the $\alpha$, $\beta$ chromophores and 93 cm$^{-1}$ for the chromophores in the B800 ring. The steady-state spectra were modeled together with modified Redfield theory outlined by Novoderezhkin *et al.* [40] with the additional high frequency modes included by addition of discrete oscillators to the line broadening function.

## 2.2 Dynamics

While the electronic degrees of freedom are of interest to us, we must also introduce the effect of the surrounding protein and solvent environment. The bath Hamiltonian phenomenologically describes the stochastic fluctuations in the environment that cause electronic energy gap fluctuations in the chromophores, and hence line broadening. The system-bath interaction is taken to be linear and can be related to the reorganization energy, which is half the Stokes shift – the difference in energy between the peaks of the absorption spectra and emission spectra. The full Hamiltonian reads

$$H = H_S + H_B + H_{SB}. \qquad (1)$$

To model energy transfer in LH2 we choose the scaled hierarchical equations of motion (HEOM) [47] which, assuming a Gaussian spectral density, can simulate the propagation of electronic energy transfer without treating the system-bath interaction in a perturbative manner. We note that the method will not capture many important features of energy transfer, in particular the role of intramolecular vibrations (vibronic lineshapes) that play an important role in the spectral overlap [39]. Nevertheless, the method yields a useful qualitative model of energy transfer dynamics and, importantly, does not require formal distinction between the B800 and B850 chromophores.

The scaled version of HEOM developed by Shi *et al.* [47] has been proven to converge faster than earlier formulations [48]. Twenty unique realizations of the system Hamiltonian with diagonal disorder were generated and used for the simulations. A Drude spectral density was employed, and the system-bath coupling for each site is assumed to be the same such that

$$J(\omega) = \left(\frac{2E_R\gamma}{\hbar}\right)\frac{\omega}{\omega^2 + \gamma^2} \qquad (2)$$

where $\gamma$ is the the Drude decay constant, the inverse of which determines the time scale over which non-equilibrium phonon dynamics happen [13]. By employing this spectral density, the bath correlation function can be rewritten as

$$C(t > 0) = \sum_{\kappa=0}^{\infty} c_\kappa \cdot e^{-v_\kappa t} \qquad (3)$$

With the Matsubara frequencies $v_0 = \gamma$ and $v_\kappa = 2\kappa\pi/\beta\hbar$ for $\kappa \geq 1$. The constants $c_\kappa$ are defined as

$$c_0 = E_R\gamma\hbar\left[\cot\left(\frac{\beta\hbar\gamma}{2}\right) - i\right]$$

$$c_\kappa = \frac{4E_R\gamma}{\beta\hbar} \cdot \frac{v_\kappa}{v_\kappa^2 - \gamma^2} \text{ for } \kappa \geq 1 \qquad (4)$$

After applying the Ishizaki-Tanimura [49] truncation scheme and using the scaled HEOM approach [47] we can write the scaled density operator as

$$\begin{aligned}
\frac{d}{dt}\rho_n = &-\frac{i}{\hbar}[H_e, \rho_n] - \sum_{i=1}^{N} n_i \gamma \cdot \rho_n \\
&+ i\sum_{i=1}^{N}\sqrt{(n_i+1)|c_0|}\left[\mathcal{V}_i, \rho_{n_i^+}\right] \\
&- \sum_{i=1}^{N}\sum_{\kappa=1}^{\infty}\frac{c_\kappa}{v_\kappa} \cdot [\mathcal{V}_i, [\mathcal{V}_i, \rho_n]] \\
&- \sum_{i=1}^{N}\sum_{\kappa=1}^{\infty}\frac{c_\kappa}{v_\kappa} \cdot [\mathcal{V}_i, [\mathcal{V}_i, \rho_n]] \\
&+ i\sum_{i=1}^{N}\sqrt{n_i/|c_0|}\left(c_0\mathcal{V}_i\rho_{n_i^-}\right. \\
&\left. - c_0^*\rho_{n_i^-}\mathcal{V}_i\right)
\end{aligned} \qquad (5)$$

where $n$ is a global index that is a set of non-negative integers $n \equiv \{n_1, n_2, ..., n_N\}$ with $0 \leq \sum_j n_j \leq \mathcal{H}$ where $\mathcal{H}$ is the hierarchy at which the equations are truncated. The global index $n$ is used to label the set of density operator $\rho_n$, with $\rho_0$ as the reduced density operator and all others are the auxiliary density operators that are corrections to the system-bath interaction. $n_{j\pm}$ changes the number $n_j$ to $n_j + 1$. We chose a reorganization energy of $65\,\text{cm}^{-1}$ which was based on the B800 peak stokes shift measurement of $130\,\text{cm}^{-1}$. $\gamma^{-1}$ is the bath relaxation time, and $\gamma/c$ was set to be $53\,\text{cm}^{-1}$, as reported by Scholes and Fleming [39].

## 2.3 Measures of Delocalization

Recently Smyth and Scholes [35] developed analytical measures of multipartite delocalization in mixed states with a single excitation. These measures can detect hierarchies of multipartite entanglement, allowing one to get a precise measurement of the delocalization length of an excitation in a system undergoing decoherence. The restriction to the single excitation subspace means that coherence is a sufficient and not just a necessary condition for the presence of entanglement. This in turn allows us to borrow concepts from multipartite entanglement, such as hierarchies of separability. By determining the number of entangled states one is able quantify the extent and strength of the delocalized excitation.

Previous analytical measures would only detect 2-body delocalization [15,16,31], and often solely for pure states. One exception is the set of measures derived by Scholak *et al*. [20], but again, these were for purely coherent systems only. The work in the present paper builds on our earlier work [25] which reviewed the measures commonly employed in the field, from the Inverse Participation Ratio, a measure of 2-body delocalization, to the tangle, a measure of 2-body entanglement. Along with this review the connection between these measures was explored, revealing an interesting relationship. The total 2-body entanglement in a system can be expressed as a function of the purity of the state, and the second order statistical moment (i.e. the IPR):

$$E_2(\rho) = \text{Tr}(\rho^2) - M_2(\rho). \qquad (6)$$

We can also rewrite this in terms of the bipartite measure $\tau_2(\rho) = 1 - M_2(\rho)$, and measure the distance of a state $\rho$ from it's closest separable state $\sigma$ such that

$$E_2(\rho) = \tau_2(\rho) - \tau_2(\sigma). \qquad (7)$$

We can then extend this idea to higher levels of entanglement and delocalization such that we measure the distance of a state from its closest state $\sigma$ with $k-1$ entanglement:

$$E_k(\rho) = \tau_k(\rho) - \tau_k(\sigma) \qquad (8)$$

Determining the correct reference states is crucial so that these measures are effective; the process is detailed in Smyth and Scholes [35].

In general [50] $\tau_k$ can be calculated from

$$\tau_k = \sum_{i_0=1}^{N-k+1} \rho_{i_0 i_0} \sum_{i_1=i_0+1}^{N-k+2} \rho_{i_1 i_1} \cdots \sum_{i_{k-1}=i_{k-2}+1}^{N} \rho_{i_{k-1} i_{k-1}}. \qquad (9)$$

# 3 Delocalization length in LH2

Using the delocalization measures Eqs 6-9 one is able to precisely measure delocalization length of a model system of LH2. Here we define the delocalization length as the largest level of multipartite entanglement. For example, in a system with no more than tripartite entanglement, the delocalization length is simply 3. It is important to note however that as with all measurements, these delocalization measures are subject to error. The advantage of these measures is that one can not only tell the number of sites participating in an excitation but the strength of their interaction. Thus these measures give an added dimension to the term "delocalization length". Moreover, as we will see later, it is also worth considering the effective delocalization length. This is the number of correlated sites that actually appear to influence aspects of energy transfer.

There are several factors that affect the delocalization length; chief among them is the strength of decoherence, which will serve to reduce coherence regardless of the basis chosen. Within the site basis (the basis chosen here) the early-time delocalization length also depends strongly on the initial conditions (e.g. initial size of the exciton), while the steady-state delocalization length depends on the delocalization of the energy eigenstates and their level of degeneracy. For example, in LH2 the delocalization length is constrained by the size of the spectrally distinct B800 and B850 rings.

First let us examine the delocalization length predicted by three different simulations (using the Hamiltonian

with zero disorder) with the different initial states: (i) an excitation starting on a single site in the B800, (ii) an exciton with the highest B800 population, and (iii) an exciton with the highest B850 population. Figs. 1-4 contain plots for each simulation that detail the time-dependent delocalization length, bipartite entanglement evolution (denoted by E2) and, where applicable, multipartite entanglement evolution (denoted by E3-E18). Note that the simulations presented in this section are obtained using the Hamiltonian with zero disorder and that any static disorder or inhomogenous broadening would serve to reduce the delocalization length.
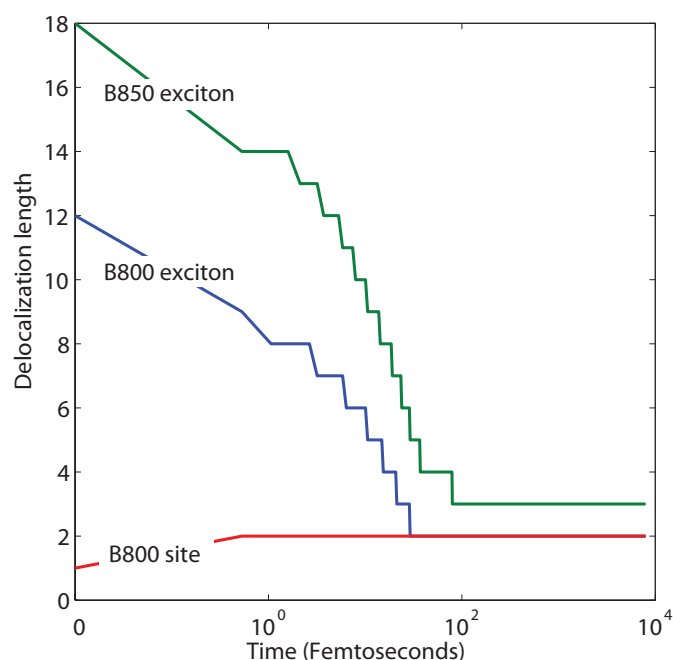


**Fig. 1.** Time-dependent delocalization length for three different simulations, the most populous B800 exciton, the most populous B850 exciton and a single B800 site as the initial state. The time scale is logarithmic. These were run using the Hamiltonian with zero disorder.
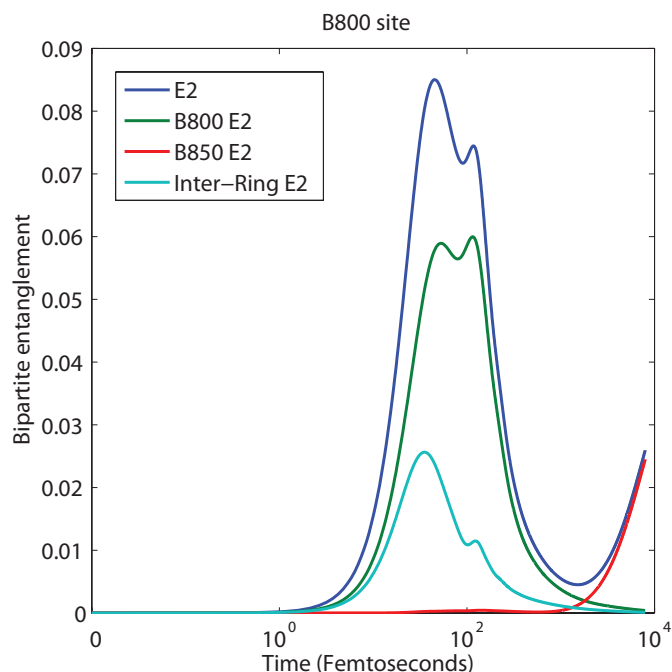
**Fig. 2.** Time-dependent bipartite entanglement for a model LH2 complex with a single chromophore as the initial state (note the scale of the y-axis which indicates weak bipartite entanglement).

Consider the case of an excitation starting on a single site in B800 and travelling to the B850 ring, as plotted in fig. 1. As expected the initial delocalization length is just 1, this increases to and remains at a length of 2 for the remainder of the simulation. The advantage of using entanglement based measures in measuring delocalization is that we can see where the excitation is delocalized. As we can see in fig. 2 the initial growth of the entanglement is within the B800 ring and between the B850 and B800 ring, rather than within the B850 ring itself. At later times the excitation is almost exclusively delocalized within the B850 ring. However the level of bipartite delocalization at all times never extends beyond a value of 0.1, indicating the mixed state consists of weakly correlated pairs. We can conclude that the size of the initial exciton has limited the delocalization length, while the strength of this bipartite entanglement is also constrained by the coupling within the B800 ring and between the B850 and B800 rings.

Now consider an excitation starting on an eigenstate with the highest B800 population (99.5%). While initially the state has a delocalization length of 12 (fig. 1), the multipartite entanglement levels for $E10 - E12$
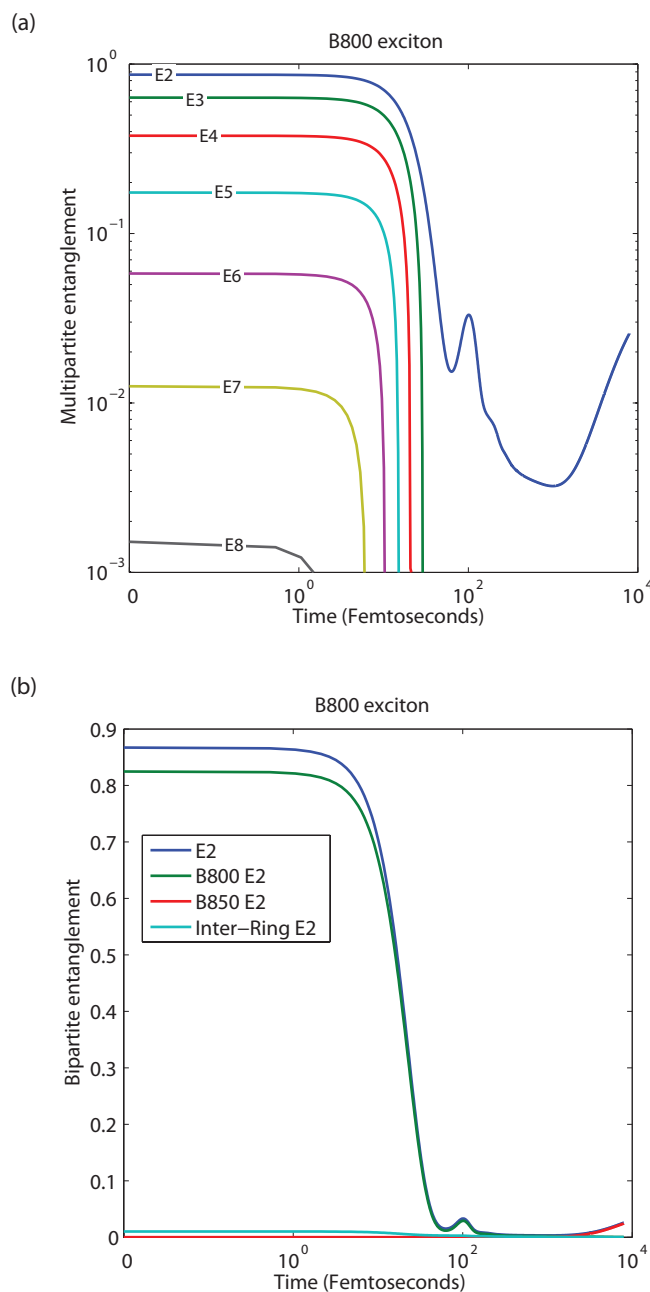


**Fig. 3 (a)** Multipartite entanglement evolution for the B800 exciton as the initial state. Both axes are in log scale**. (b)** Time-dependent bipartite entanglement for a model LH2 complex with the B800 exciton as the initial state. Bipartite entanglement is broken down into intra and inter ring components.

are orders of magnitude smaller than E9, meaning there is a small but unlikely chance that the excitation could be found in the B850 ring at $t = 0$. These levels are so small they don't even appear in our logarithmic plot in fig. 3a. This is due to the fact that the two rings in LH2 are spectrally very distinct, although here some small overlap between the rings has occurred within this system eigenstate. Within 30 fs all multipartite

delocalization vanishes and the excitation rapidly localizes to just 2 sites. In fig. 3b we can see that the bipartite entanglement was initially mainly within the B800 ring and was quite strong, while the long term dynamics show that the excitation localizes to the weakly entangled dimer pairs within the B850 ring.

Finally let us examine the case of an excitation starting on an eigenstate with the highest B850 population (99.99%). Again, due to the spectral distinction between rings, the delocalization length is limited to the B850 ring only. While the initial delocalization length is 18 sites (fig. 1), the exciton chosen is not evenly delocalized across the B850 ring, as such the 13-partite entanglement and above is too weak to plot. The excitation also quickly localizes—this time to three sites—within about 80 femtoseconds. This larger thermalized delocalization length can be attributed to the stronger coupling within the B850. Much like the B800 case, higher levels of entanglement are extremely weak and don't appear in fig. 4a. Fig. 4b shows that initially the excitation was almost maximally entangled, indicating near perfect delocalization, with each chromophore having equal probability of excitation. There is no visible B800 or inter-ring entanglement indicating energy transfer is restricted to within the B850 ring. This is expected as the B800 ring lies energetically above the B850 ring.

From these models one can draw some interesting conclusions. Delocalization in the B800 ring is surprisingly long lasting, with strong bipartite entanglement in the first 100 femtoseconds, and weak bipartite entanglement lasting throughout the whole simulation. This contradicts the often touted "monomeric" nature of the B800 ring. While typically the inter-ring entanglement is relatively weak, it nevertheless has an effective role. In a later section it is posited that inter-ring entanglement is associated with fast transfer between rings. At very short timescales we see evidence of multipartite entanglement across entire rings, while at longer timescales the delocalization length reaches a steady value of 2 or 3 sites. An interesting question then to ask is: does this early stage multipartite entanglement play a role in EET in the LH2 light harvesting complex
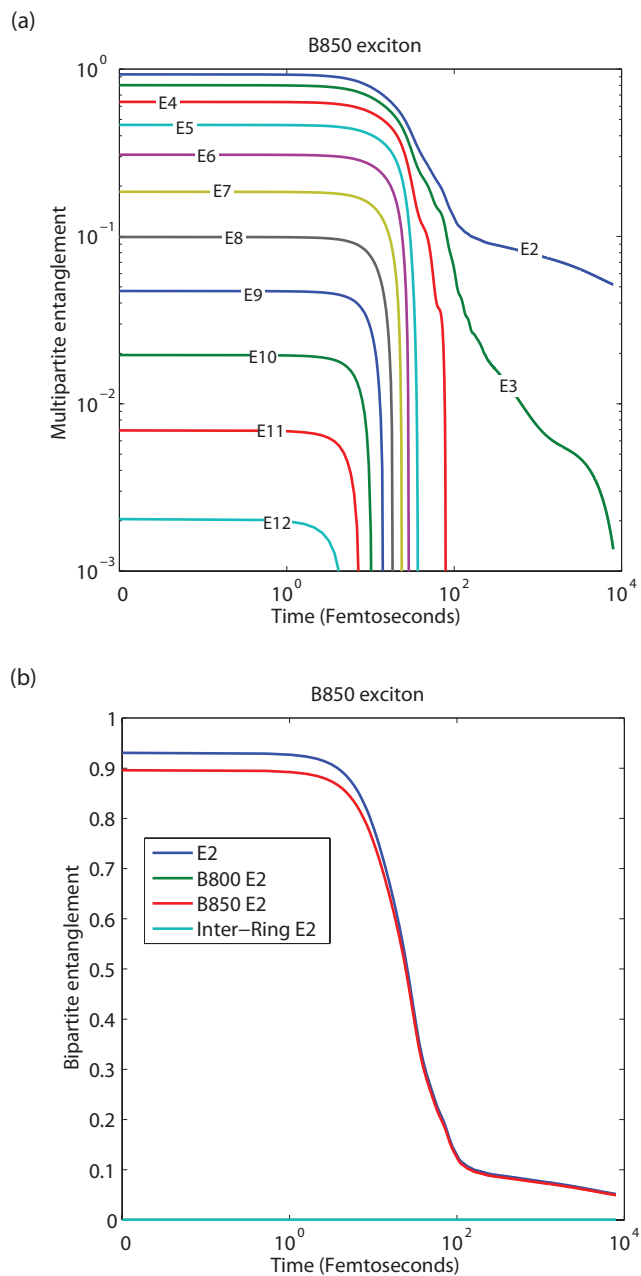


**Fig. 4 (a)** Multipartite entanglement evolution for the B850 exciton as the initial state. Both axes are in log scale**. (b)** Time-dependent bipartite entanglement for a model LH2 complex with the B850 exciton as the initial state. Bipartite entanglement is broken down into intra and inter ring components.

A similar study by Strümpfer and Schulten [49] determined that the steady state delocalization length in the B850 ring was approximately 12 sites. Although similar methods to those employed in this paper were used in simulating EET, the measure of delocalization they employed gave larger values. This delocalization measure [50] has been demonstrated to be a less

effective tool for measuring delocalization [25]. While the results presented in our work may also seem at odds with some experimental estimations of the delocalization length that posit that the delocalization length extends over the entire B850 ring [53-55], the consensus in the field is that excitation is delocalized in the B850 ring over $4 \pm 2$ sites [57-61].

# 4 Physical distance of correlation

While we present here an accurate measure of the delocalization length, the term itself is somewhat misleading. One might be tempted to think that a delocalization length of 2 means that an excitation is shared across two neighbouring sites. As we will see in this section, this is not necessarily the case. In this analysis, the three simulations from the Hamiltonian (without disorder) from section 3 are employed to study the spatial distance between correlated chromophores. In fig. 5 the physical distance between entangled chromophores is plotted in two different ways. First we consider the distance between two maximally correlated sites at a given point in time. Fig. 5a plots the distance between these two sites. By examining the strongest correlation we are essentially examining the distance between the most likely pair of sites that share a delocalized excitation.

We also consider the "average distance of correlation". This value, plotted in fig. 5b, is the distance between every possible pair in LH2 weighted by their corresponding levels of bipartite entanglement. It's interesting to note that for the case where a single site is set as the initial state, one can see an increase in the
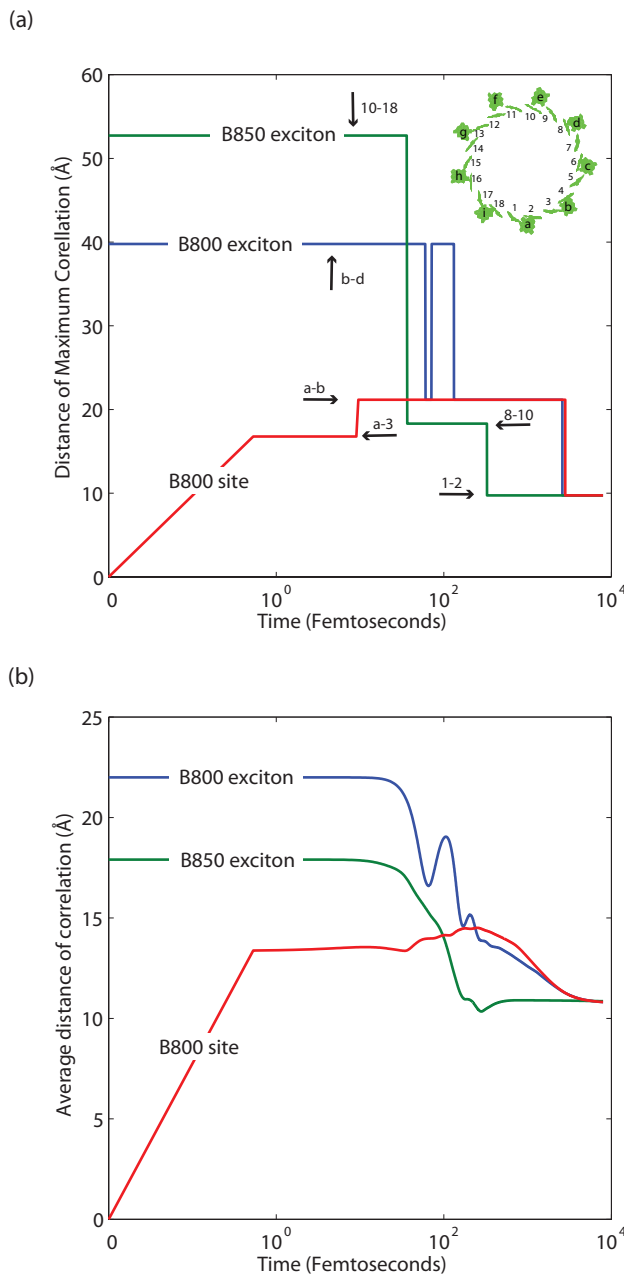


**Fig. 5 (a)** Distance between sites with the strongest correlation at a given time. Note the increase in distance in the case of the initial state being a B800 site. Each distance is labeled with a corresponding pair of sites, with the labeling a-i representing the B800 sites and 1-18 representing the B850 sites, as shown in the inset illustration of the LH2 complex. The subunits are grouped as a-1-2, b-3-4, etc. **(b)** Average distance between sites weighted by the strength of their respective correlations. Distance units are in Ångstroms.

distance between correlated pairs at later times. The increasing curve in fig. 5b is a combination of relatively strong correlations between neighbouring B800 sites and increasing inter-ring correlations. With an excitation beginning on the B800 exciton, it is

somewhat surprising that for the majority of the simulation the B800 sites b & d, followed by d & e (same distance as a & b labeled), have the strongest bipartite entanglement. In the case of an excitation starting on the B850 exciton, initially the strongest correlation is between two sites (10 & 18) on opposite sides of the B850 ring, even after the delocalization length reduces to 5 sites. The strongest correlation quickly reduces to next-nearest neighbour (8 & 10) and then nearest neighbour (9 & 10). In fig. 5b one sees an unusual beating in the B800 case, though most of this can be attributed to beating in the inter-site coherence. In all cases the distance in both plots reduces to the distance within the $\alpha - \beta$ dimer pair in the B850, indicating that the excitation is physically localizing.

# 5 Delocalization and transfer rates using disordered Hamiltonians

Now let us examine energy transfer across the two rings in LH2. Using 20 disordered LH2 Hamiltonians we look at two types of initial states: a single site on the B800 ring, and the exciton with the highest B800 population. In reality the structure of the LH2 light harvesting complex will not be perfectly symmetric, and no two LH2 complexes will be exactly the same. Therefore by adding disorder to the Hamiltonian one can gain a more realistic picture of energy transfer in LH2, as well as an opportunity to take a more statistical approach to transfer rates and entanglement levels within ensembles of these complexes.

Examining figs. 6a and 6b one sees a wide distribution of inter-ring transfer rates for the single site and B800 exciton case respectively. Both plots show the fastest and slowest systems, along with the mean $\mu$ and standard deviation $\sigma$. The transfer rate $R$ is calculated as the rate of change in the B850 ring population $P$ weighted by the B800 population. While as expected the

fastest (slowest) simulation has a larger (smaller) than average rate of transfer, note also that the faster the predicted energy transfer the more sustained the initial growth of transfer rate.

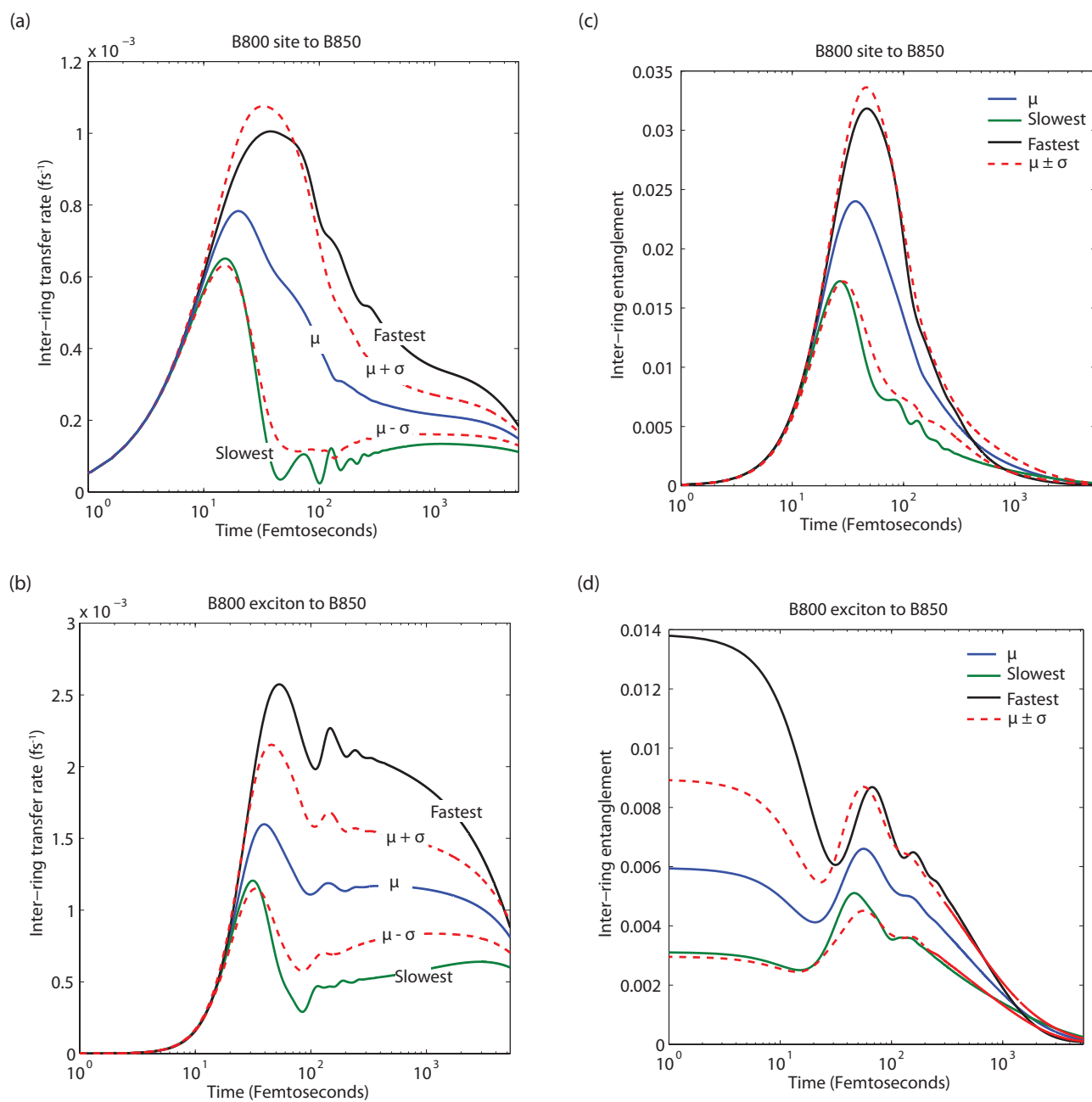$$R = \frac{\frac{dP(t)}{dt}}{(1 - P(t))} \qquad (10)$$

(a)



(c)



(b)



(d)



**Fig. 6 (a-b)** Inter-ring transfer rate for systems with **(a)** a single site as the initial state and **(b)** the B800 exciton given as an initial state. The transfer rate for the fastest growing population (iteration 12 for **(a)** and iteration 3 for **(b)**) and the slowest growing population (iteration 2) are plotted, along with the ensemble average ($\mu$) and standard deviation ($\mu \pm \sigma$).
**(c-d)** Inter-ring entanglement for systems with **c)** a single site as the initial state and **(d)** the most populous B800 exciton given as an initial state. The fastest growing population (iteration 12 for **c)** and iteration 3 for **(d)**) and the slowest growing population (iteration 2) are plotted, along with the ensemble average ($\mu$) and the standard deviation ($\mu \pm \sigma$).
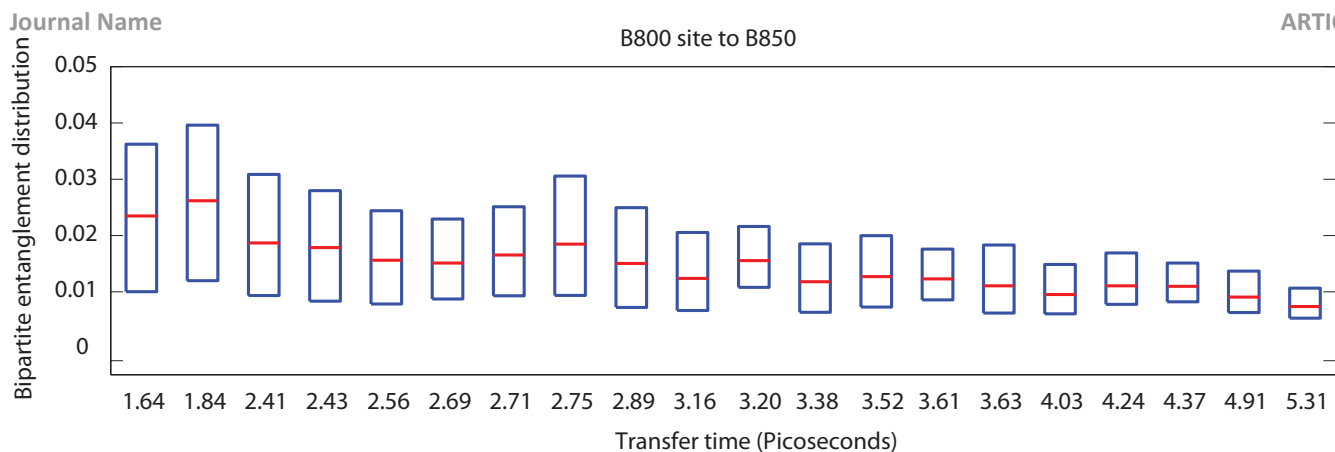
**Fig. 7** Box plot of bipartite entanglement distribution over time versus transfer times for 20 disordered simulations with a single B800 site as the initial state. The red line in each data point indicates the median value, while the blue box indicates the 25th and 75th percentiles. Note the narrowed entanglement distribution for simulations that predict longer transfer times, as well as smaller median entanglement. The transfer time is defined as the time it takes for the B850 ring to reach majority population.
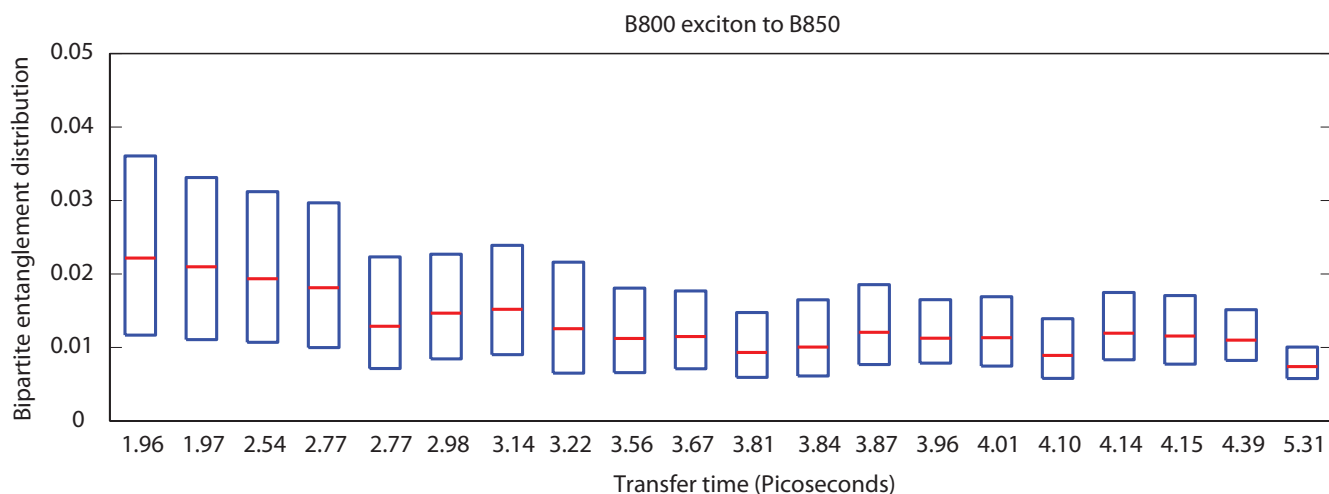


**Fig. 8** Box plot of bipartite entanglement distribution over time versus transfer times for simulations with the most populous B800 exciton. The red line in each data point indicates the median value, while the blue box indicates the 25th and 75th percentiles. Again note the smaller entanglement distribution and median for longer transfer times.

Table 1 Correlation between transfer time ($t_T$) and entanglement. The angular brackets denote lifetime average. The transfer time is defined as the time it takes for the B850 ring to reach majority population

|  | $t_T$ | $\langle E2 \rangle$ | $\langle E3 \rangle$ | $\langle E4 \rangle$ | $\langle E5 \rangle$ | $\langle E6 \rangle$ | $\langle E7 \rangle$ | $\langle E8 \rangle$ | $\langle E9 \rangle$ |
|---|---|---|---|---|---|---|---|---|---|
| $t_T$ | 1.00 | **-0.94** | **-0.05** | **-0.01** | **0.04** | **0.07** | **0.09** | **0.09** | **0.09** |
| $\langle E2 \rangle$ | -0.94 | 1.00 | -0.12 | -0.14 | -0.13 | -0.14 | -0.14 | -0.13 | -0.13 |
| $\langle E3 \rangle$ | -0.05 | -0.12 | 1.00 | 0.94 | 0.81 | 0.68 | 0.60 | 0.55 | 0.54 |
| $\langle E4 \rangle$ | -0.01 | -0.14 | 0.94 | 1.00 | 0.96 | 0.86 | 0.79 | 0.75 | 0.74 |
| $\langle E5 \rangle$ | 0.04 | -0.13 | 0.81 | 0.96 | 1.00 | 0.96 | 0.92 | 0.89 | 0.88 |
| $\langle E6 \rangle$ | 0.07 | -0.14 | 0.68 | 0.86 | 0.96 | 1.00 | 0.99 | 0.98 | 0.98 |
| $\langle E7 \rangle$ | 0.09 | -0.14 | 0.55 | 0.75 | 0.89 | 0.98 | 1.00 | 1.00 | 1.00 |
| $\langle E8 \rangle$ | 0.09 | -0.13 | 0.55 | 0.75 | 0.89 | 0.98 | 1.00 | 1.00 | 1.00 |
| $\langle E9 \rangle$ | 0.09 | -0.13 | 0.54 | 0.74 | 0.88 | 0.98 | 1.00 | 1.00 | 1.00 |

In both groups of initial states (single site and most populous B800 exciton) all but a single realization of the LH2 realizations reach over 50% B850 population before the simulation was stopped (roughly 5.3 picoseconds). Interestingly enough, in both cases the under-performing model comes from the same disordered Hamiltonian. Also of note is that, in the case of the initial state being a single site, simulation 12 was the fastest, while it was the second fastest in the case of the initial state being the B800 exciton. We see similar trends when we examine the inter-ring entanglement in these simulations, as plotted in figs. 6c and 6d. In this plot the fastest (slowest) simulations have higher (lower) than average inter-ring entanglement and fall within range of the standard deviation. This seems to suggest a relationship between rapid energy transfer and high levels of bipartite entanglement. Let us now further examine if entanglement, whether bipartite or multipartite, is correlated with energy transfer rate.

Table 1 details the correlation strength between the lifetime average (average entanglement while it exists) of various levels of entanglement ($\langle E2 \rangle$ to $\langle E9 \rangle$) and the transfer time (defined as the time taken to reach a B850 majority) for the realizations with the most populous B800 exciton as the initial state. In the two cases that did not reach a majority the transfer time is changed to the lifetime of the simulation, given that those B850 populations were reasonably close to 50%. The lifetime average of entanglement is employed because of the short lifetime of the multipartite entanglement; otherwise these values would be skewed towards zero. The correlation strength calculated here is the Pearson correlation coefficient of the two normalized distributions.

For bipartite entanglement there is a near perfect ($-0.936$) anti-correlation with the transfer times, meaning longer transfer times occur in systems with lower bipartite entanglement. For the multipartite entanglement however, there is not any effective

correlation, meaning the short-lived multipartite entanglement has no impact on inter-ring energy transfer times. Indeed the bipartite entanglement shows no real correlation with the different levels of multipartite entanglement, though they themselves have strong inter-correlations. This is because of the short-lived lifetime of the multipartite entanglement; in a system with longer lived multipartite entanglement one would expect stronger correlations between transfer times and multipartite entanglement.
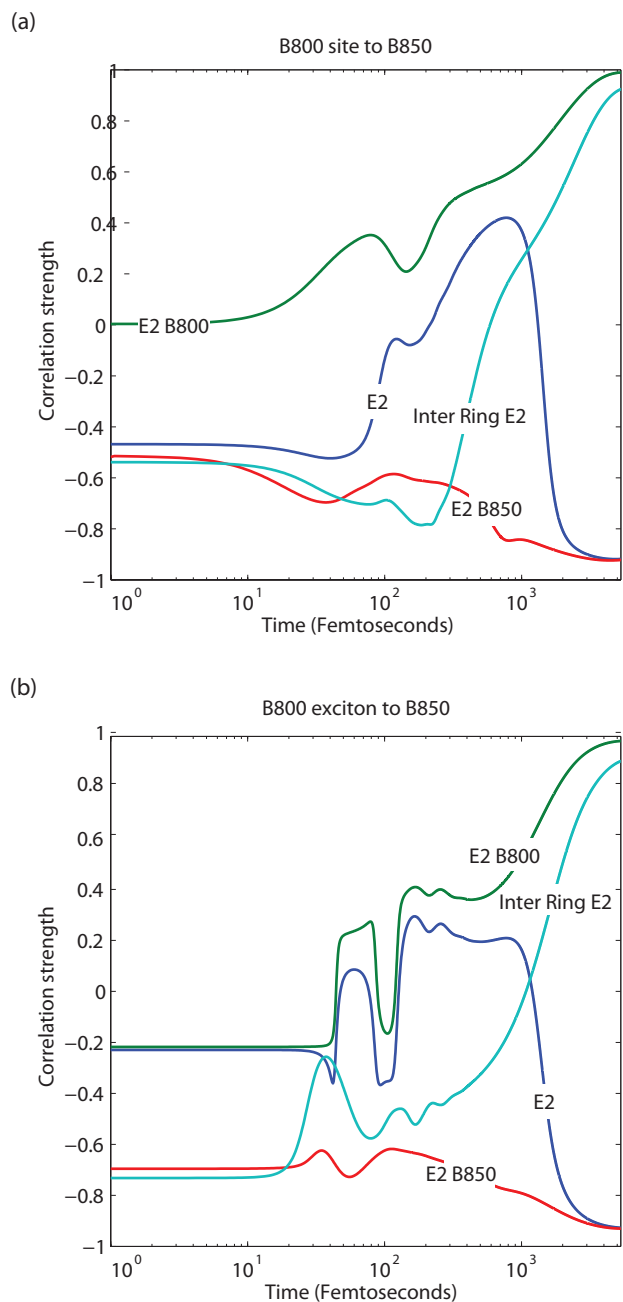
(a)



(b)



**Fig. 9.** Correlation strength between bipartite entanglement, inter-

ring entanglement and intra-ring entanglement, and transfer time for simulations with **(a)** a single B800 site as the initial state and **(b)** the B800 exciton as the initial state. The Transfer time is defined as the time it takes for the B850 ring to reach majority population.

A good way to visualize the correlation between bipartite entanglement and transfer times is with a boxplot. Figs. 7 and 8 contain boxplots of the bipartite entanglement distribution over time versus the transfer times for each realization, in both the case of a single site as an initial state and the B800 exciton as an initial state. In both cases there tends to be a smaller median bipartite entanglement for longer transfer times, as well as a smaller distribution of bipartite entanglement. This corresponds well with the anti-correlation value of $-0.94$.

Now let us examine these correlations in further detail, once again by splitting the bipartite entanglement into entanglement within the B800 ring, the B850 ring, and between the two rings. Fig. 9 plots the time dependent correlation strength between the transfer time and each of these types of bipartite entanglement. The bipartite entanglement within the B800 ring evolves into being strongly correlated with the transfer time in both cases. Likewise the B850 bipartite entanglement becomes more anti-correlated with transfer times in both cases. This makes sense, as higher levels of B850 entanglement require higher B850 population levels, much like lower B800 entanglement can be the result of lower B800 population. In the case of the initial state being a single site, the bipartite entanglement in B800 begins completely uncorrelated with the transfer time; whereas it has a weak anti-correlation when the initial state is a B800 exciton.

The inter-ring entanglement is the most telling, however. At early times after the dynamics are photo-initiated, the inter-ring entanglement is moderately anti-correlated with the transfer time, before progressing to being nearly completely correlated. This tells us the importance of early time coherence between the two rings, and how inter-ring coherence at later times can be a hindrance. This result is similar to that of [25] where the authors determined that coherence within the B800

complex increases the rate of inter-ring energy transfer in LH2.

Crucially our results show that inter-ring coherence plays a much stronger role than intra-ring coherence in the B800 ring. From the perspective of Generalized Förster Theory this has implications. Our work indicates that the seemingly reasonable assumption of uncorrelated B800 to B850 energy transfer misses interesting components of the dynamics. That is, energy transfer from one aggregate to another is sped up by coherence at early transfer times. The wider implication of this result is that even in cases of rather weak electronic coupling (*ca.* 30 cm$^{-1}$) coherence modifies energy transfer dynamics.

## 6. Energy gradient and transfer rates

Delocalization is a consequence of strong coupling in light-harvesting complexes such as LH2. Another consequence of strong electronic coupling is that it leads to a splitting in the eigen-energies. This splitting lifts any degeneracies and creates an energy gradient. This in turn ensures "downhill" energy transfer from the B800 ring, to the B850 ring, and on to the LH1 complex. This raises the question: are faster transfer rates due to a steeper energy gradient? Furthermore, is the correlation between delocalization and transfer rates then simply due to the causal relationship between the energy gradient and transfer rates?

Here we present the correlation strengths between the energy gradient, the mean bipartite entanglement and the transfer times for states with an excitation on the exciton with the highest B800 population. We treat the energy gradient in two ways: as the slope of the linear fit of the full eigenvalue spectrum of the disordered Hamiltonian, $\Delta_f$, as well as the slope of the linear fit of the available eigenvalue spectrum $\Delta_a$ (i.e. from the energy of the initial state down to the lowest eigenvalue).

**Table 2.** Comparison of energy gradient and delocalization correlations with transfer times

| | $\langle E2 \rangle$ | $\Delta_f$ | $\Delta_a$ |
|---|---|---|---|
| Transfer time | -0.94 | -0.58 | 0.09 |

As we can see in table 2, the mean bipartite entanglement still has the strongest correlation with the transfer time, followed by $\Delta_f$ and then $\Delta_a$. It is curious that the full energy gradient is somewhat correlated with transfer times, while available energy gradient is not. Owing to the weak correlation between $\Delta_a$ and the transfer times it is clear that delocalization is not simply an artifact of downhill energy transfer in a coupled system. Instead delocalization appears to play an active role in assisting energy transfer via constructive interference. This is further supported by the observation that while the eigenstates of LH2 can be distinctly associated with the B800 and B850 rings, the level of delocalization within these eigenstates does not correlate with the transfer time as strongly as the entanglement *between* the rings.

## Conclusion

Not only is the role of quantum effects in photosynthetic energy transfer an open question, but so too is the scale of its very presence. Here we have attempted to quantify the role of coherence in energy transfer by employing a carefully constructed Hamiltonian, a distribution of simulations using the most reliable quantum master equations available, as well as the most precise delocalization measurements. Whether one is analyzing simulated or experimental data, the most effective tools need to be employed. The delocalization measures we employed in this study provide such accuracy, and will be essential when experimental techniques such as state tomography become feasible for complex systems. Though the initial delocalization length of an excitation in LH2 may extend over an entire ring, the steady-state delocalization length is over just 2 or 3 sites. Moreover, multipartite delocalization is so short-lived that it has seemingly no role in inter-ring energy transfer at ambient temperature.

Having determined the scale of delocalization we were able to focus on its role. A clear correlation between inter-ring transfer times and bipartite entanglement was established. This result indicates that the *effective* delocalization length in LH2 is no greater than 2 sites, for the entire duration of EET. Further analysis of the various types of bipartite entanglement (inter and intra-ring) determined that inter-ring coherence plays a pivotal role in energy transfer in LH2, far more than intra-B800, in contrast with previous studies [26]. This result has implications for methods such as Generalied Förster Theory that assume uncorrelated B800 to B850 energy transfer—an approximation that seems entirely reasonable given that the electronic coupling is only $\sim$20–30 cm$^{-1}$. However, how calculations show that energy transfer from one aggregate to another is sped up by coherence at early transfer times. The wider implication of this result is that even in cases of rather weak electronic coupling coherence modifies energy transfer dynamics.

While multipartite entanglement apparently plays no role in B800-B850 energy transfer, it is not to say that such entanglement is irrelevant in photosynthetic energy transfer. Plenty of other systems such as the FMO complex would benefit from the deeper analysis that these multipartite delocalization measures provide. Even a study of B850 to LH1 energy transfer could yield some surprising results. Whether one is analyzing simulated or experimental data, the most effective tools need to be employed. These delocalization measures provide such accuracy, and will be essential when obtaining the system density matrix becomes a reality. This can be obtained through experimental techniques such as state tomography. Alternatively, a judicious time-dependent measure of system entropy coupled with site population statistics could be sufficient [11]. A recent letter by Tempelaar *et al.* [62] suggests site coherence could be measured using time-resolved spectroscopy. It would be interesting to see if such a measure could be applied to LH2 and if similar conclusions to those presented here would be made.

It remains a challenge to work out how to measure delocalization incisively with experiments. At present, the results of simulated data help point the way for devising new measurements. Here our results suggest that, rather than focusing on the delocalization length,

any measurement of electronic coherence is effective enough in determining the role of quantum coherence in energy transfer in LH2.

## Acknowledgments

## References

[1]  E. Schrödinger, *What is Life? The Physical Aspects of the Living Cell*, Cambridge University Press, Cambridge, 1944.

[2]  G. McDermott, S. M. Prince, A. A. Freer, A. M. Hawthornthwaite-Lawless, M. Z. Papiz, R. Cogdell and N. W. Isaacs, *Nature*, 1995, **374**, 517–521.

[3]  G. S. Engel, T. R. Calhoun, E. L. Read, T.-K. Ahn, T. Mancal, Y.-C. Cheng, R. E. Blankenship and G. R. Fleming, *Nature*, 2007, **446**, 782–6.

[4]  G. Panitchayangkoon, D. Hayes, K. Fransted, J. R. Caram, E. Harel, J. Wen, R. E. Blankenship and G. S. Engel, *Proc. Natl. Acad. Sci.*, 2010, **107**, 12766–12770.

[5]  G. Panitchayangkoon, D. V. Voronine, D. Abramavicius, J. R. Caram, N. H. C. Lewis, S. Mukamel and G. S. Engel, *Proc. Natl. Acad. Sci. U. S. A.*, 2011, **108**, 20908–12.

[6]  E. Collini, C. Y. Wong, K. E. Wilk, P. M. G. Curmi, P. Brumer and G. D. Scholes, *Nature*, 2010, **463**, 644–647.

[7]  D. B. Turner, R. Dinshaw, K.-K. Lee, M. S. Belsley, K. E. Wilk, P. M. G. Curmi and G. D. Scholes, *Phys. Chem. Chem. Phys.*, 2012, **14**, 4857–74.

[8]  D. B. Turner, K. E. Wilk, P. M. G. Curmi and G. D. Scholes, *J. Phys. Chem. Lett.*, 2011, **2**, 1904–1911.

[9]  S. J. Harrop, K. E. Wilk, R. Dinshaw, E. Collini, T. Mirkovic, C. Y. Teng, D. G. Oblinsky, B. R. Green, K. Hoef-Emden, R. G. Hiller, G. D. Scholes and P. M. G. Curmi, *Proc. Natl. Acad. Sci.*, 2014, **111**, E2666–75.

[10]  G. S. Schlau-Cohen, T. R. Calhoun, N. S. Ginsberg, E. L. Read, M. Ballottari, R. Bassi, R. van Grondelle and G. R. Fleming, *J. Phys. Chem. B*, 2009, **113**, 15352–63.

[11]  G. D. Scholes and C. Smyth, *J. Chem. Phys.*, 2014, **140**, 110901.

[12]  V. Coffman, J. Kundu and W. K. Wootters, *Phys. Rev. A*, 2000, **61**, 052306.

[13]  W. Dür, G. Vidal and J. Cirac, *Phys. Rev. A*, 2000, **62**, 062314.

[14]  V. Vedral, M. B. Plenio, M. Rippin and P. L. Knight, *Phys. Rev. Lett.*, 1997, **78**, 2275–2279.

[15]  M. Sarovar, A. Ishizaki, G. R. Fleming and K. B. Whaley, *Nat. Phys.*, 2010, **6**, 462–467.

[16]  F. Fassioli and A. Olaya-Castro, *New J. Phys.*, 2010, **12**, 085006.

[17]  A. Chin, A. Datta, F. Caruso, S. Huelga and M. B. Plenio, *New J. Phys.*, 2010, **12**, 065002.

[18]  A. Ishizaki and G. R. Fleming, *New J. Phys.*, 2010, **12**, 1–12.

[19]  J. Zhu, S. Kais, A. Aspuru-Guzik, S. Rodriques, B. Brock and P. J. Love, *J. Chem. Phys.*, 2012, **137**, 074112.

[20]  T. Scholak, F. de Melo, T. Wellens, F. Mintert and A. Buchleitner, *Phys. Rev. E*, 2011, **83**, 021912.

[21]  F. Caruso, A. Chin, A. Datta, S. Huelga and M. B. Plenio, *Phys. Rev. A*, 2010, **81**, 062346.

[22]  K. Brádler, M. M. Wilde, S. Vinjanampathy and D. B. Uskov, *Phys. Rev. A*, 2010, **82**, 062310.

[23]  D. a. Mazziotti, *J. Chem. Phys.*, 2012, **137**, 074117.

[24]  J. Cai, S. Popescu and H. J. Briegel, *Phys. Rev. E*, 2010, **82**, 021921.

[25]  C. Smyth, F. Fassioli and G. D. Scholes, *Philos. Trans. A. Math. Phys. Eng. Sci.*, 2012, **370**, 3728–49.

[26]  Y.-C. Cheng and R. J. Silbey, *Phys. Rev. Lett.*, 2006, **96**, 028103.

[27]  H. Hossein-Nejad, C. Curutchet, A. Kubica and G. D. Scholes, *J. Phys. Chem. B*, 2011, **115**, 5243–53.

[28]  M. Mohseni, P. Rebentrost, S. Lloyd and A. Aspuru-Guzik, *J. Chem. Phys.*, 2008, **129**, 174106.

[29]  P. Rebentrost, M. Mohseni, I. Kassal, S. Lloyd and A. Aspuru-Guzik, *New J. Phys.*, 2009, **11**, 033003.

[30]  Q. Tan and L. M. Kuang, *Sci. China Physics, Mech. Astron.*, 2012, **55**, 1541–1548.

[31]  D. Thouless, *Phys. Rep.*, 1974, **13**, 93–142.

[32]  R. Jimenez, S. N. Dikshit, S. E. Bradforth and G. R. Fleming, *J. Phys. Chem.*, 1996, **100**, 6825–6834.

[33]  H. Fidder, J. Knoester and D. A. Wiersma, *J. Chem. Phys.*, 1991, **95**, 7880.

[34]  V. I. Novoderezhkin, R. Monshouwer and R. van Grondelle, *J. Phys. Chem. B*, 1999, **103**, 10540–10548.

[35]  C. Smyth and G. D. Scholes, *Phys. Rev. A*, 2014, **90**, 032312.

[36]  O. Gühne, G. Tóth and H. J. Briegel, *New J. Phys.*, 2005, **7**, 229–229.

[37]  R. E. Blankenship, *Molecular Mechanisms of Photosynthesis*, Blackwell Science Ltd, Oxford, England, 1st edn, 2002.

[38] V. Sundström, T. Pullerits and R. van Grondelle, *J. Phys. Chem. B*, 1999, **103**, 2327–2346.

[39] G. D. Scholes and G. R. Fleming, *J. Phys. Chem. B*, 2000, **104**, 1854–1868.

[40] V. I. Novoderezhkin, A. B. Doust, C. Curutchet, G. D. Scholes and R. van Grondelle, *Biophys. J.*, 2010, **99**, 344–52.

[41] M. Z. Papiz, J. Preskill, T. Howard, R. Cogdell and N. W. Isaacs, *J. Mol. Biol.*, 2003, **326**, 1523–1538.

[42] M. J. Frisch, G. W. Trucks, H. B. Schlegel, G. E. Scuseria, M. A. Robb, J. R. Cheeseman, G. Scalmani, V. Barone, B. Mennucci, G. A. Petersson and others, *Gaussian Inc., Wallingford, CT*, 2009.

[43] A. D. Becke, *J. Chem. Phys.*, 1993, **98**.

[44] P. J. Stephens, F. J. Devlin, C. F. Chabalowski and M. J. Frisch, *J. Phys. Chem.*, 1994, **98**, 11623–11627.

[45] R. A. Kendall, T. H. Dunning and R. J. Harrison, *J. Chem. Phys.*, 1992, **96**.

[46] J. B. Foresman, M. Head-Gordon, J. A. Pople and M. J. Frisch, *J. Phys. Chem.*, 1992, **96**, 135–149.

[47] Q. Shi, L. Chen, G. Nan, R.-X. Xu and Y. Yan, *J. Chem. Phys.*, 2009, **130**, 084105.

[48] J. Zhu, S. Kais, P. Rebentrost and A. Aspuru-Guzik, *J. Phys. Chem. B*, 2011, **115**, 1531–7.

[49] Y. Tanimura, *J. Phys. Soc. Japan*, 2006, **75**, 082001.

[50] T. Scholak, *PhD thesis*, Albert-Ludwigs-Universitat Freiburg, 2011.

[51] J. Strümpfer and K. Schulten, *J. Chem. Phys.*, 2009, **131**, 225101.

[52] T. Meier, V. Chernyak and S. Mukamel, *J. Phys. Chem. B*, 1997, **101**, 7332–7342.

[53] D. Leupold, H. Stiel, K. Teuchner, F. Nowak, W. Sandner, B. Ücker and H. Scheer, *Phys. Rev. Lett.*, 1996, **77**, 4675–4678.

[54] V. Nagarajan, R. G. Alden, J. C. Williams and W. W. Parson, *Proc. Natl. Acad. Sci.*, 1996, **93**, 13774–9.

[55] N. R. . S. Reddy, R. . Picorel and G. J. Small, *J. Phys. Chem.*, 1992, **96**, 6458–6464.

[56] V. I. Novoderezhkin and A. P. Razjivin, *FEBS Lett.*, 1995, **368**, 370–2.

[57] R. Monshouwer, M. Abrahamsson, F. van Mourik and R. van Grondelle, *J. Phys. Chem. B*, 1997, **101**, 7241–7248.

[58] T. Pullerits, M. Chachisvilis and V. Sundström, *J. Phys. Chem.*, 1996, **100**, 10787–10792.

[59] M. Chachisvilis, O. Kühn, T. Pullerits and V. Sundström, *J. Phys. Chem. B*, 1997, **101**, 7275–7283.

[60] M. Dahlbom, T. Pullerits, S. Mukamel and V. Sundström, *J. Phys. Chem. B*, 2001, **105**, 5515–5524.

[61] V. Nagarajan, E. Johnson, J. C. Williams and W. W. Parson, *J. Phys. Chem. B*, 1999, **103**, 2297–2309.

[62] R. Tempelaar, F. C. Spano, J. Knoester and T. L. C. Jansen, *J. Phys. Chem. Lett.*, 2014, **5**, 1505–1510.

## Notes and references

[a] Department of Physics, University of Toronto, Toronto, Canada..

[b] Department of Chemistry, Princeton University, Washington Rd, Princeton NJ 08544, USA

1 Citations here in the format A. Name, B. Name and C. Name, *Journal Title*, 2000, **35**, 3523; A. Name, B. Name and C. Name, *Journal Title*, 2000, **35**, 3523.